Progress In Electromagnetics Research, Vol. 141, 291–307, 2013

A SHAPED-BEAM SERIES-FED APERTURE-COUPLED STACKED PATCH ARRAY ANTENNA

Lei Qiu[1, *], Sheng Shui Wang[1], Hui Ying Qi[1], Fei Zhao[2], Shun Lian Chai[1], and Jun Jie Mao[1]

[1]College of Electronic Science and Engineering, National University of Defense Technology, Changsha 410073, China

[2]Southwest Electronics and Telecommunication Technology Research Institute, Chengdu 610041, China

Abstract—A shaped-beam series-fed aperture-coupled stacked patch array antenna at X-band is presented. To improve the array bandwidth, two-port aperture-coupled stacked patch antennas, which are suitable for the series-fed array configuration, are presented as the radiating elements. To offer the pattern design and optimization progresses more flexibility, a uniformly spaced array configuration is applied in the shaped-beam pattern design, instead of the conventional nonuniformly spaced array configuration. The experimental results show that, in a 7.6% bandwidth, the main beam shape of the array maintains in good agreement with the design goal, and the side lobe level maintains lower than −18 dB.

1. INTRODUCTION

Due to its key features, such as ease of construction, low cost, light weight, low profile and ease of surface mounting, microstrip antenna [1, 2] has been widely applied in the radar and communication areas, and has become an important member of the antenna family.

In a low profile microstrip array antenna, the signal may be distributed via a corporate feed network or a series feed kind [3]. Microstrip corporate-fed arrays are usually applied in the circumstances where wide bandwidth is needed [4]. They can offer a wider bandwidth than series-fed arrays, because the signals all travel

Received 28 May 2013, Accepted 6 July 2013, Scheduled 18 July 2013

* Corresponding author: Lei Qiu (xwnaruto@163.com).

along equal or approximately equal paths to the radiating elements, which avoids the phase dispersion in the operating band due to different signal path lengths. However, they surfer huge feed lost since the total length of the feed paths are very long [5].

On the other hand, the microstrip series-fed arrays can offer better antenna efficiency performance, because the total feed line lengths are inherently minimized, which leads to the reduction of line radiation and dissipation losses [6]. Furthermore, their aperture distributions, so as the far field patterns, can be controlled in a more convenient and precise way [7–10].

Before the 1980s, most of the microstrip series-fed arrays were constructed in the form of monolithic arrays [6]. But this kind of antenna structure usually suffered the spurious radiation from the feed lines, which degraded the pattern performances, such as raising the side lobe level [11, 12], or causing distortion of the main beam shape in some shaped-beam pattern designs [13].

There were several proposed solutions to this spurious radiation problem, e.g., applying mirror configuration of the array elements [7], or placing the feed network behind the ground plane [14, 15], etc.. Among these, the application of the aperture coupled microstrip antenna proposed in 1985 [16] offered a good solution to this problem. Its feed line was on the back side of the antenna, shielded by the ground plane, so the spurious leakage radiation from the transmission lines were eliminated. In addition, it left quite enough space for the feed network, which offered more flexibility to the network design. After that, lots of works about the aperture coupled microstrip array antennas had been carried out with good array performances achieved [17–20].

In [18], the authors designed a dual-polarized microstrip series-fed linear traveling-wave array consists of four-port aperture-coupled cross-patch elements and a two-port radiating matched load. The array was configured in a nonuniformly spaced traveling-wave array form, in which the radiating amplitude and phase of each element can be controlled by tuning the length of the coupling slot and the distances between the elements, respectively. The simulated pattern results showed low sidelobe level properties and low cross-polarization features at the principle plane. In [20], the authors designed a large aperture circularly polarized shaped-beam array, which also used the same kind of elements in [18]. The measured results showed good impedance matching performance, and a cosecant-squared pattern with some distortion of the main beam.

However, the resonant property of the aperture-coupled patch element is determined by the resonator consisted of the slot-patch

pair, which has only one sharp resonance peak on its frequency curve. This will cause mainly two problems with such kind of arrays. Firstly, due to the sharpness of the resonance peak, the radiation amount of each element, so as the array distributions, will change rapidly with the frequency varying. This will narrow the pattern bandwidth of the arrays. Secondly, the resonance peak will shift away from the center frequency point when the slot length or the patch dimensions change. Thus, the coupling coefficient at the center frequency will vary more rapidly as these parameters changing, which cause the aperture distribution to be sensitive to fabrication errors. Additionally, the nonuniformly spaced array configuration has its own drawback to implement the shaped-beam patterns. The interrelation of the radiating phases and element positions in a nonuniformly spaced series-fed array will make some particular shaped-beam patterns hardly to be obtained, especially when optimization progress is needed to compensate the mutual coupling between the elements (since the element position have to be changed during the phase optimization process, which will distort the pattern performance).

In this paper, a shaped-beam series-fed aperture-coupled stacked patch array antenna, which applies a uniformly spaced traveling-wave array configuration, is presented. Instead of the aperture-coupled patch elements, two-port aperture-coupled stacked-patch (ASP) antennas have been designed as the array elements and the conventional ASP antenna [21] is applied as the radiating matched load. The double-resonance property of the aperture-coupled stacked-patch maintains in the two-port form, which improves the pattern bandwidth and offers the array a better tolerance to the fabrication errors. In addition, for the reason of implementing the uniformly spaced array configuration, microstrip phaseshifters have been placed between each ASP element and the phase distribution of the array is obtained by tuning their phases. This configuration offers more flexibility in the design and optimization progresses of the array radiation pattern. At last, it should be mentioned that, a metal box has been added behind the array to eliminate the spurious radiation caused by the bends in the microstrip phaseshifters.

The organization of this paper is as follows. The two-port and the terminal radiating ASP antenna elements are featured in Section 2. The microstrip phaseshifters applied in the array are also described in this section. Then, in Section 3, the array structure and the design method is described. In Section 4, the experimental results of a linear array are presented and discussed.

2. DESIGN OF THE RADIATING ELEMENTS AND THE PHASESHIFTERS

The array is designed with the aid of Ansoft High Frequency Structure Simulator (HFSS) which is based on FEM (Finite element method).

2.1. Two-port ASP Antenna Element

The structure of the two-port ASP antenna element is depicted in Fig. 1. Just as the conventional ASP antennas, the element consists of two stacked patches, a dogbone shape coupling slot [22], a microstrip feed line and three dielectric substrate layers to support them. As the energy passes through the microstrip feed line under the antenna, part of it will be coupled through the slots to the lower patch, then to the upper patch, and finally radiating to the free space. The coupling level, so as the radiation amount of each element, can be controlled by tuning the slot length of the two-port ASP.

The permittivity ε_r of all the three substrates is 2.55, and the thickness of them are fixed as follows: $h_1 = 1.016\,\text{mm}$, $h_2 = 1.524\,\text{mm}$, $h_3 = 0.762\,\text{mm}$. The upmost substrate which contains the upper

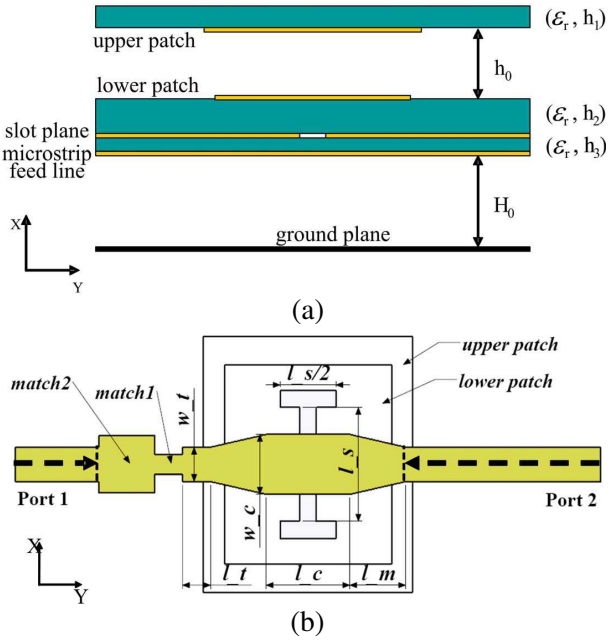

Figure 1. Two-port ASP antenna element. (a) Side view, (b) bottom view.

radiating patches at its bottom also acts as a protective cover of the antenna. The thickness of the bottom substrate contains the microstrip feed line is chosen to be thin to eliminate the surface wave modes in the substrate, which otherwise would decrease the gain and degrade the pattern performance of the array. A metal box has been placed at the bottom of the antenna to eliminate its back radiation (only the bottom plane of the box is shown in Fig. 1(a)). The thickness (H_0) of the metal box is 10 mm ($0.35\lambda_{10.5\,\mathrm{GHz}}$), which is higher enough to avoid its influence to the feed line.

As shown in Fig. 1(b), the microstrip line right below the coupling slot has been set to be wider than the main feed line of the array to further improve the coupling coefficients of the elements. And two mirrored changes have been added to the two end of this wide microstrip line section to improve the impedance matching condition. Two-section tuning slits have been added forward to each element in order to gain a wide band impedance matching. The lengths of the tuning slits are fixed, and the widths of them are tuned to get matching according to different slot lengths. The dashed arrows in Fig. 1(b) mean that the S parameters of the two-port ASP are calculated according to the planes at the ends of these arrows.

All the fixed structure parameters of the two-port ASP elements are listed in Table 1, where w_up and l_up are the width (X direction) and the length (Y direction) of the upper patch, w_down and l_down are the width and the length of the lower patch, w_slot is the width of the coupling slot, l_match1 and l_match2 are the lengths of the two sections of the tuning slits. Those values of the fixed parameters in Table 1 have been initialized from design experiences of microstrip lines, microstrip line coupled slots and conventional microstrip patches, then optimized though simulation.

Table 1. Fixed structure parameters of the two-port ASP (unit: millimeters).

w_up	9	w_slot	0.6	w_t	1
l_up	7.5	l_c	3	l_t	1
w_down	8	w_c	2.1	l_match1	1
l_down	7	l_m	2	l_match2	2

The simulated return losses and transmission phases of the two-port ASP elements with three different slot lengths are shown in Fig. 2. It can be observed that all these elements have obtained a return loss below -20 dB in a 14% bandwidth around the center frequency. And Fig. 2(b) shows that, the transmission phase curves versus frequency

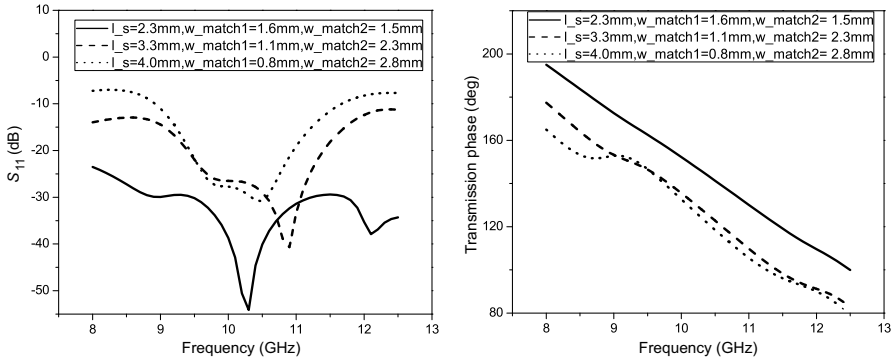

Figure 2. Simulated return losses and transmission phases of the two-port ASP with three different slot lengths. (a) Return losses, (b) transmission phases.

are approximately linear curves around the center frequency point, with a maximum $\pm 5^\circ$ difference from the linear curves as the frequency varies in a 30% bandwidth. Therefore, the phase distribution of the array can be assured to change in an approximately linear way within a broad bandwidth. As is well known, the linear phase change of the elements will only leads to a pointing direction shift of the radiation pattern at the principal plane. The phase curves also show that, the transmission phases of different slot lengths are slightly different, which will be considered during the phase design process in Section 3.

The coupling coefficient of the two-port ASP, which represents its radiation capability and can be directly used in the array design process, is defined as

$$C = \frac{1 - \left|S_{11}^2\right| - \left|S_{21}^2\right|}{\left|S_{21}^2\right|} \tag{1}$$

Fig. 3 shows the coupling coefficients of the two-port ASP antennas with three different slot lengths. Two resonance peaks can be clearly observed from each coupling coefficient curve. These well tuned double-resonant properties have flattened the coupling coefficients curves, with a maximum $\pm 8\%$ ripple in a 14% bandwidth. It means the radiation amount of each element will still approximately satisfy the amplitude distribution designed at the center frequency while the frequency varies in a broad bandwidth, thus the pattern bandwidth of the array can be broadened. In the mean time, it also can be observed that the coupling coefficients grow bigger as the slot length arises. Therefore, the amplitude distribution of the array can be achieved through controlling the slot lengths of the elements. The radiation patterns of the two-port ASP at the center frequency are plotted in Fig. 4.

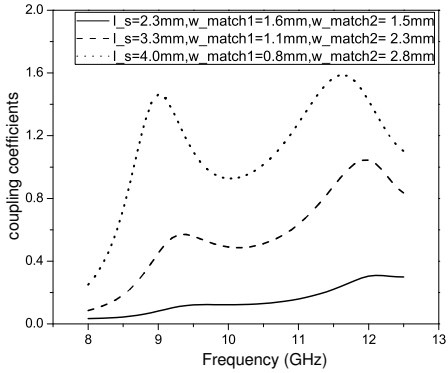

Figure 3. Coupling coefficients of the two-port ASP with three different slot lengths.

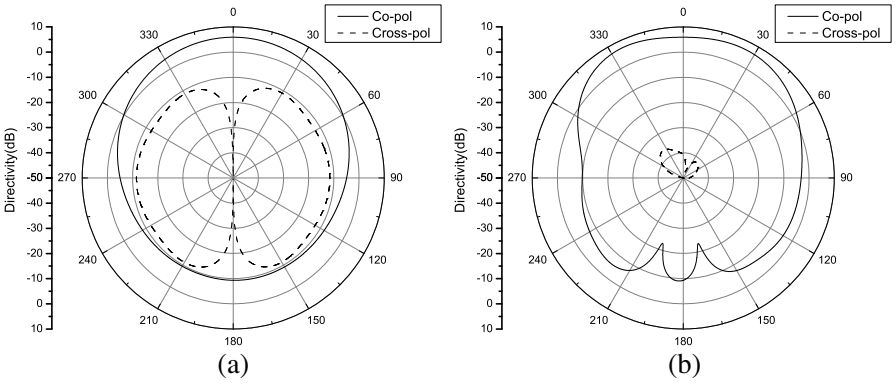

Figure 4. Radiation patterns of the two-port ASP at the center frequency, with $l\_s = 3.3\,\text{mm}$, $w\_match1 = 1\,\text{mm}$, $w\_match2 = 2\,\text{mm}$. (a) X-Z plane, (b) Y-Z plane.

At last, for the sake of the array design, the coupling coefficient curve and the transmission phase curve versus the slot length at the center frequency point have been simulated and shown in Fig. 5.

2.2. One-port ASP Radiating Matched Load

A conventional one-port ASP antenna is placed at the end of the array as a radiating matched load, which has mainly two functions: one is to act as a matched load of the traveling wave array; the other is as a radiation element which has its own contribution to the radiation pattern. This radiating matched load configuration [18] makes use of the power which would usually be waste in a matched load in a conventional traveling wave array [23], therefore improves the efficiency of the array.

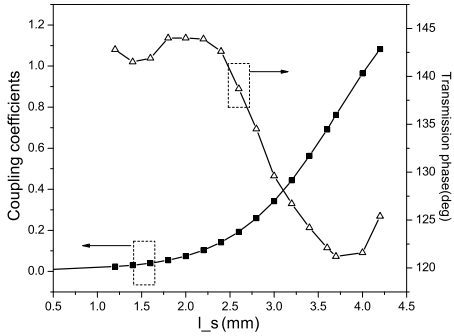

Figure 5. Coupling coefficient curve and transmission phase curve of the two-port ASP at the center frequency.

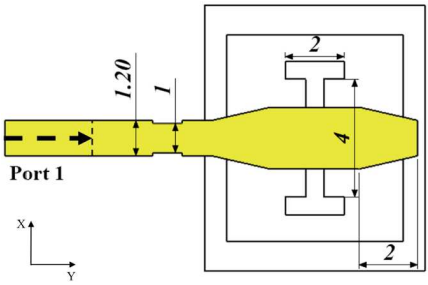

Figure 6. Structure of the one-port ASP radiating matched load (bottom view, unit: millimeters).

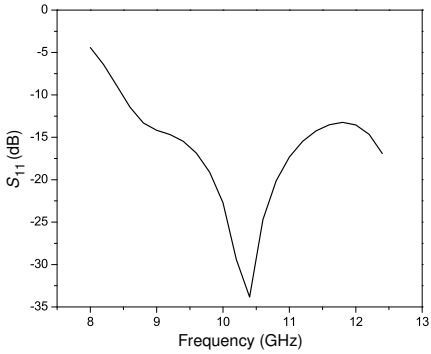

Figure 7. Return loss of the one-port ASP.

As shown in Fig. 6, the only difference of the structure of the one-port ASP from the two-port ASP is that, instead of port 2, it consists of a microstrip open end at its right side. All the structure parameters of the one-port ASP are fixed, and their values are as the same as the parameters of two-port ASP listed in Table 1, except the slot length is 4 mm, $w\_match1 = 1$ mm, $w\_match2 = 1.2$ mm.

Figure 7 shows its simulated return loss. It is observed that the element has been tuned to have a 2 : 1 VSWR bandwidth bigger than 38% around the center frequency.

2.3. Microstrip Phaseshifters

The element spacing of the array has been set to be equal. Unlike the way of designing a nonuniformly spaced linear array, in which

the radiating phases of the antenna elements are usually controlled by tuning the element spaces, here microstrip phaseshifters are placed between the radiating elements to control the radiating phases.

There are two kinds of microstrip phaseshifters used in the array, both shown in Fig. 8. The one with inclined bends in Fig. 8(a) is to achieve the phase shift from 0° to 50°, with respect to a 6 mm long straight microstrip line. The other with square bends shown in Fig. 8(b) is to achieve bigger phase shift, which is from 50° to 150°, also with respect to the 6 mm microstrip line. Both of the phaseshifters are controlled by changing *length_x*. The reason for this two structure choice is that, when *length_x* is too big, the matching condition of the inclined bend phaseshifter will get worse. On the contrary, the square bend phaseshifter can not stand a small *length_x*.

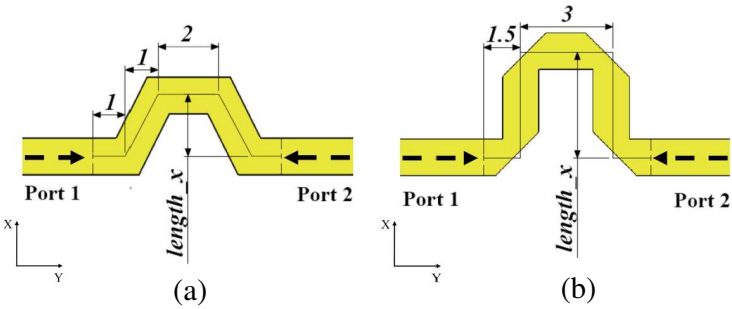

Figure 8. Structures of the two kinds of microstrip phaseshifters (unit: millimeters). (a) With inclined bends, (b) with square bends.

It must be noted that, the bends in the microstrip phaseshifters will cause some spurious radiation and insertion loss to the array. Although a metal box has been placed behind the array, which can suppress the spurious radiation adequately, the insertion loss will still be inevitable, since the spurious radiation can not be utilized efficiently through this configuration. This is the main drawback for applying the microstrip phaseshifters, and can be observed from the comparison of the simulated and measured gains of the array in Section 4. The simulated return losses of the two kinds of phaseshifters are both lower than −20 dB in their entire tuning range in a 30% bandwidth. And their insertion losses, which include the metal and material losses, are from 0.15 dB to 0.4 dB in their entire tuning range. For the sake of the array design, the phase shift curves of the two kinds of phaseshifters versus *length_x* have been simulated and shown in Fig. 9.

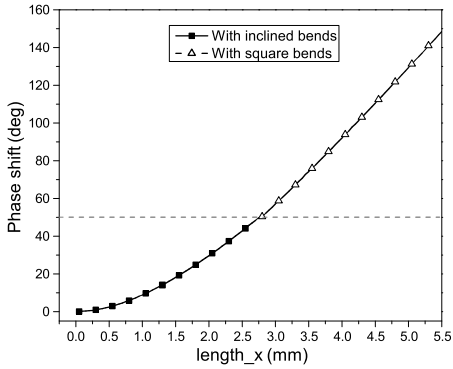

Figure 9. Phase curves of the two kinds of microstrip phaseshifters at the center frequency.

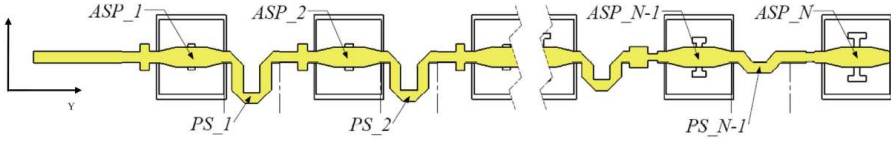

Figure 10. Structure of the array (bottom view).

3. ARRAY STRUCTURE AND DESIGN METHOD

Figure 10 shows the structure of the array, which consists of 15 two-port ASP elements, 15 followed microstrip phaseshifters and a one-port ASP radiating load. The element spacing should be sufficiently large to leave enough space for the phaseshifters; meanwhile, to restrict the array length, it should not be too large. In this paper, the element spacing has been set as 17 mm according to these considerations.

The particle swarm method [24, 25] has been applied to synthesize the ideal shaped pattern in Fig. 11. The distribution is shown in Fig. 12, and the theoretically calculated pattern result is shown in Fig. 11 for the sake of comparison.

Here the conventional design method of traveling-wave arrays has been applied to achieve the synthesized amplitude distribution. The radiating power of the one-port ASP radiating load is set as P_N, and the radiating power of element n is calculated as

$$P_n = P_N \times f_n^2 / f_N^2 \tag{2}$$

where f_n and f_N denote the amplitude of the nth element and the end load. The coupling coefficient of each element can be calculated as

$$C_n = \frac{P_n}{P_{n+1} + P_{n+2} + \ldots + P_N} \tag{3}$$

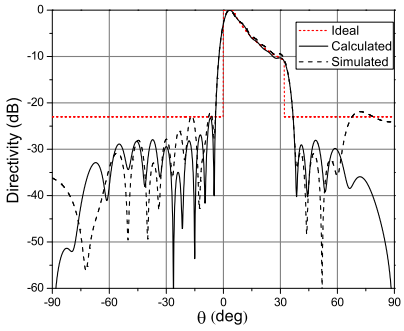

Figure 11. Ideal, calculated and the simulated shaped patterns at the principle plane.

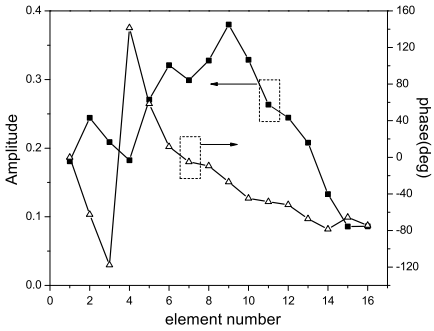

Figure 12. Distribution of the shaped-beam pattern.

Then the corresponding slot length of each element can be deduced from the coupling coefficient curve in Fig. 5. And also the phase delay of each element can be calculated out according to the transmission phase curve.

According to the uniformly spaced array configuration, the element positions are no longer limitation to the phase distribution. Therefore, the phase distribution can be achieved simply by setting the phase shift of each phaseshifter as

$$Phase_n = (angle_{n+1} - angle_n) - Phase_{slot\_n} \tag{4}$$

where $angle_n$ and $Phase_{slot\_n}$ mean the needed radiating phase and the transmission phase of the nth element. Then the corresponding structure parameters of the phaseshifters can be calculated out according to the phase shift curves in Fig. 6.

It is worth mentioned that, since the mutual coupling effect has not been considered in the design process, the actual aperture distribution of the array with the designed structure parameters will be different from the design goal. Here, a trial-error optimization method [26] has been applied to optimize the structure parameters. Again, since the interrelation of the radiating phases and element positions has gone, the phase optimization can be achieved by simply optimizing the $length\_x$ of the phaseshifters, without considering the influence of the element position change.

The final optimized array structure has been modeled and simulated by using HFSS, and the simulated pattern result at the center frequency is shown in Fig. 11. It can be observed that, the simulated shaped-beam pattern gets a excellent beam shape, which is nearly identical to the calculated one, and the simulated side lobe level is lower than -22 dB.

4. EXPERIMENTAL RESULTS AND DISCUSSIONS

The fabricated substrate layers of the array are shown in Fig. 13. The material of the substrate layers is the ARLON AD255 with $\varepsilon_r = 2.55$, $\tan\delta = 0.002$ at 10.5 GHz. The upper patches are printed on the bottom layer of substrate 1. Substrate 2 contains the lower patches on its top layer, and the coupling slots on its bottom layer. The microstrip feed line is printed on the bottom layer of substrate 3. Two rows of vias have been fabricated around the lower pathes on substrate 2, which can be observed in Fig. 13, and pads have been printed on the top layer of substrate 3 corresponding to the positions of these vias. Substrate 2 and substrate 3 are finally soldered together through these vias and pads on them. It is a pity that the slots layer has not been taken picture before the soldering process.

A photo of the array is shown in Fig. 14. The air layer between the stack patches is supported by the metal disks also shown in the photo.

The simulated and measured return loss curves in Fig. 15 show that the measured one has slightly shifted to higher frequency, probably

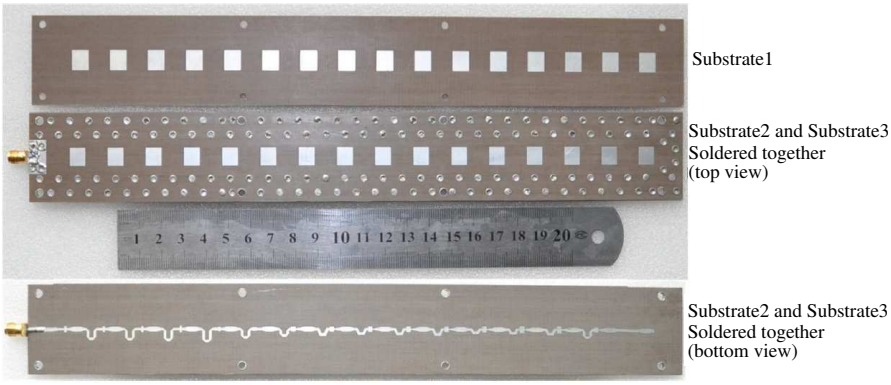

Figure 13. The fabricated substrate layers.

Figure 14. Photo of the array.

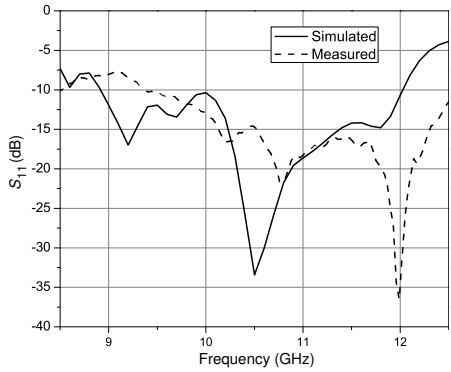

Figure 15. Simulated and measured return loss of the array.

due to the inaccurate control of the thickness of the air layer between the two stacked patches, which has slightly changed the resonance property of the elements. It can be observed that the measured 2 : 1 VSWR bandwidth is about 30%, while the previous work in [18] only achieved a bandwidth of about 7%.

The measured patterns of the array are shown in Fig. 16. It can be observed that, over a bandwidth of 7.6%, although the beam pointing direction shifts as the frequency varies, the array maintains a good beam shape which only get a ± 1 dB ripple and is in good agreement with the design goal. The measured side lobes have raised up to at most -18 dB over the entire operation band. Quite low cross-polarization levels can be observed too.

The simulated gain, without including the metal and material losses, and the measured gain are shown in Fig. 17. It can be observed that, the array features a flat measured gain response with a variation of 1.9 dB over the operating bandwidth of 7.6%. However, compared

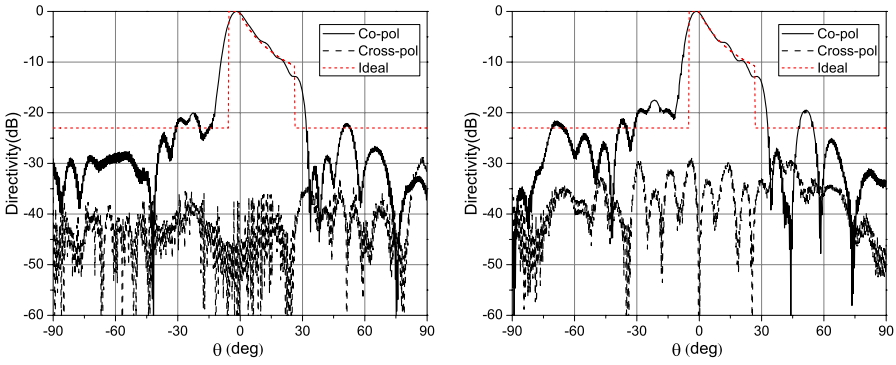

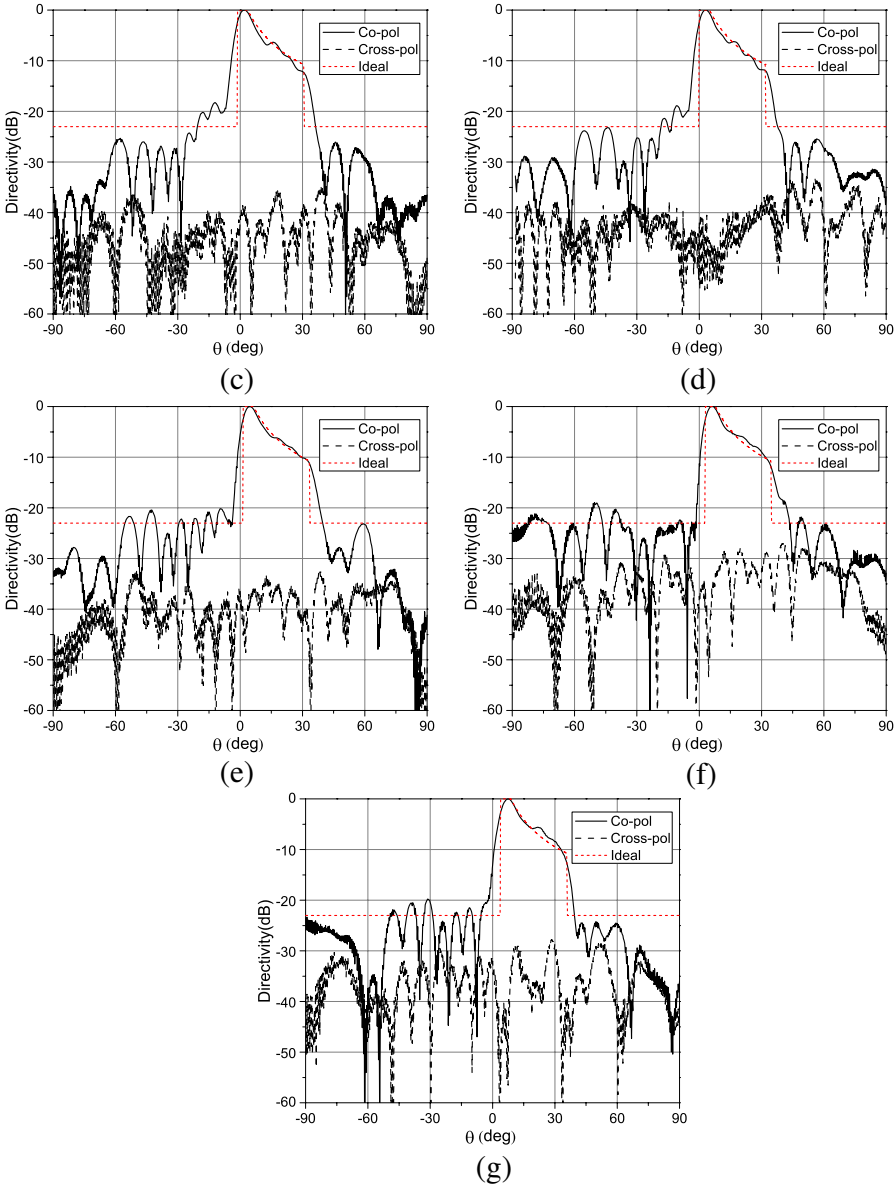

Figure 16. Measured radiation pattern of the array. (a) 10.1 GHz, (b) 10.2 GHz, (c) 10.4 GHz, (d) 10.5 GHz, (e) 10.6 GHz, (f) 10.8 GHz, (g) 10.9 GHz.

with the simulated result, the array suffers a gain drop of about 1–2.5 dB in the operation band, which is the only drawback of this design. This gain drop is mainly attributed to the metal and material losses,

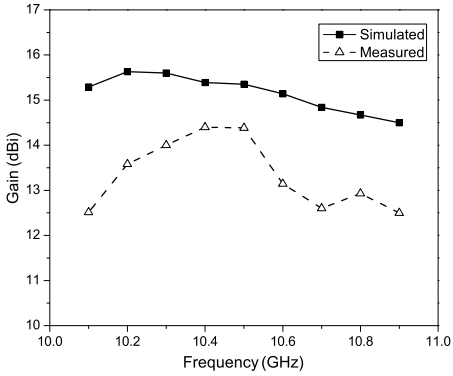

Figure 17. Simulated and measured gain of the array.

which together has been simulated to be about 0.8 dB at the center frequency. The insertion loss of the coaxial-microstrip transition, which has been measured to be about 0.2 dB, also causes a slight gain drop.

5. CONCLUSIONS

In this paper, a series-fed ASP linear array antenna has been presented for a shaped-beam pattern design. Compared with the previous work, the ASP linear array has clearly demonstrated wider operating bandwidth in terms of impedance matching, gain and radiation patterns. This bandwidth enhancement is achieved by using the proposed two-port double-resonant ASP antennas as array elements. Additionally, the array applies a uniformly spaced array configuration, which offers more flexibility in the pattern design and optimization processes than the traditional nonuniformly spaced way.

ACKNOWLEDGMENT

The authors are grateful to Dr. Liang-Feng Ye from the National University of Defense Technology for his fruitful discussions and warm help.

REFERENCES

1. Deschamps, G. A., "Microstrip microwave antenna," *3rd USAF Symp. on Antennas*, 1953.
2. Mailloux, R. J., J. Mcllvenna, and N. Kernweis, "Microstrip array technology," *IEEE Trans. on Antennas and Propagat.*, Vol. 29, No. 1, 25–38, Jan. 1981.

3. Daniel, J. P., G. Dubost, C. Terret, J. Citerne, and M. Drissi, "Research on planar antennas and arrays: structures Rayonnantes," *IEEE Antennas Propaga. Mag.*, Vol. 35, No. 1, 14–38, Jan. 1993.
4. Pozar, D. M. and D. H. Schaubert, *Microstrip Antennas, the Analysis and Design of Microstrip Antennas and Arrays*, IEEE Press, New York, 1995.
5. Hall, P. S. and C. M. Hall, "Coplanar corporate feed effects in microstrip patch array design," *IEE Proceedings*, Vol. 135, 180–186, Jan. 1988.
6. Metzler, T., "Microstrip series arrays," *IEEE Trans. on Antennas and Propagat.*, Vol. 29, No. 1, 174–178, Jan. 1981.
7. Huang, J., "A parallel-series-fed microstrip array with high efficiency and low cross-polarization," *Microwave and Optical Technology Letters*, Vol. 5, No. 5, 230–233, May 1992.
8. Babas, D. G. and J. N. Sahalos, "Synthesis method of series-fed microstrip antenna arrays," *Electronics Letters*, Vol. 43, No. 2, Jan. 2007.
9. Cui, B., J. Zhang, and X. W. Sun, "Single layer microstrip antenna arrays applied in millimeter-wave radar front-end," *Journal of Electromagnetic Waves and Applications*, Vol. 22, No. 1, 3–15, 2008.
10. He, Q.-Q. and B.-Z. Wang, "Design of microstrip array antenna by using active element pattern technique combining with Taylor synthesis method," *Progress In Electromagnetics Research*, Vol. 80, 63–76, 2008.
11. Pozar, D. M. and B. Kaufman, "Design considerations for low sidelobe microstrip arrays," *IEEE Trans. on Antennas and Propagat.*, Vol. 38, No. 8, 1176–1185, Aug. 1990.
12. Das, N. K. and D. M. Pozar, "Analysis and design of series-fed arrays of printed dipole proximity-coupled to a perpendicular microstripline," *IEEE Trans. on Antennas and Propagat.*, Vol. 37, No. 4, 435–444, Apr. 1989.
13. Jones, B. B., F. Y. M. Chow, and A. W. Seeto, "The synthesis of shaped patterns with series-fed microstrip patch arrays," *IEEE Trans. on Antennas and Propagat.*, Vol. 30, No. 6, 1106–1120, Nov. 1982.
14. Gronau, G., H. Moschuring, and I. Wolff, "Microstrip antenna arrays fed from the backside of the substrate," *Int. Symp. Antennas Propagat.*, Kyoto, Japan, 1985.
15. Vetharatnam, G., B. K. Chung, and H. T. Chuah, "Design of a

microstrip patch antenna array for airborne SAR applications," *Journal of Electromagnetic Waves and Applications*, Vol. 19, No. 12, 1687–1701, 2006.

16. Pozar, D. M., "A microstrip antenna aperture coupled to a microstrip line," *Electronics Letters*, Vol. 21, 49–50, Jan. 1985.
17. Wu, C., J. Wang, R. Fralich, and J. Litva, "Analysis of a series-fed aperture-coupled patch array antenna," *Microwave and Optical Technology Letters*, Vol. 4, No. 3, 110–113, Feb. 1991.
18. Vallecchi, A. and G. B. Gentili, "Design of dual-polarized series-fed microstrip arrays with low losses and high polarization purity," *IEEE Trans. on Antennas and Propagat.*, Vol. 53, No. 5, 1791–1798, May 2005.
19. Vallecchi, A. and G. B. Gentili, "A shaped-beam hybrid coupling microstrip planar array antenna for X-band dual polarization airport surveillance radars," *EuCAP 2007: European Conf. on Antennas Propagat.*, 1–7, Nov. 2007.
20. Guarnieri, G., G. Mauriello, G. B. Gentili, and A. Vallecchi, "Modular hybrid architecture for a large aperture circularly polarized shaped-beam antenna," *EuMA: 39th European Microwave Conference*, 755–758, 2009.
21. Croq, F. and A. Papiernik, "Stacked slot-coupled printed antenna," *IEEE Microwave and Guided Wave Letters*, Vol. 1, 288–290, Oct. 1991.
22. Zhao, F., K. Xiao, W. J. Feng, S. L. Chai, and J. J. Mao, "Design and manufacture of the wide-band aperture-coupled stacked microstrip antenna," *Progress In Electromagnetics Research C*, Vol. 7, 37–50, 2009.
23. Faffoul, G. W. and J. L. Hilburn, "Radiation efficiency of an X band waveguide array," *IEEE Trans. on Antennas and Propagat.*, 355–357, Mar. 1974.
24. Selleri, S., M. Mussetta, and P. Pirinoli, "Differentiated Meta-PSO methods for array optimization," *IEEE Trans. on Antennas and Propagat.*, Vol. 56, No. 1, 67–75, Jan. 2008.
25. Li, W. T., X. W. Shi, L. Xu, and Y. Q. Hei, "Improved GA and PSO culled hybrid algorithm for antenna array pattern synthesis," *Progress In Electromagnetics Research*, Vol. 80, 461–476, 2008.
26. Elliott, R. S., *Antenna Theory and Design*, IEEE Press, New Jersey, 2003.